Large-scale allosteric conformational transitions of adenylate kinase appear to involve a population-shift mechanism

Karunesh Arora and Charles L. Brooks III*

Department of Molecular Biology, The Scripps Research Institute, 10550 North Torrey Pines Road, La Jolla, CA 92037

Edited by Axel T. Brunger, Stanford University, Stanford, CA, and approved October 1, 2007 (received for review July 9, 2007)

Large-scale conformational changes in proteins are often associated with the binding of a substrate. Because conformational changes may be related to the function of an enzyme, understanding the kinetics and energetics of these motions is very important. We have delineated the atomically detailed conformational transition pathway of the phosphotransferase enzyme adenylate kinase (AdK) in the absence and presence of an inhibitor. The computed free energy profiles associated with conformational transitions offer detailed mechanistic insights into, as well as kinetic information on, the ligand binding mechanism. Specifically, potential of mean force calculations reveal that in the ligand-free state, there is no significant barrier separating the open and closed conformations of AdK. The enzyme samples near closed conformations, even in the absence of its substrate. The ligand binding event occurs late, toward the closed state, and transforms the free energy landscape. In the ligand-bound state, the closed conformation is energetically most favored with a large barrier to opening. These results emphasize the underlying dynamic nature of the enzyme and indicate that the conformational transitions in AdK are more intricate than a mere two-state jump between the crystal-bound and -unbound states. Based on the existence of the multiple conformations of the enzyme in the open and closed states, a different viewpoint of ligand binding is presented. Our estimated activation energy barrier for the conformational transition is also in reasonable accord with the experimental findings.

conformational change pathway | free energy calculations | ligand binding | order parameter | curve crossing

Large-scale conformational changes in proteins are often related to their function such as in signal transduction, immune response, protein folding, or enzymatic activity. These conformational changes can be induced by the interaction with other proteins or ligands. One of the key questions is to understand how the binding of a substrate leads to large-scale protein motions. Two different substrate binding mechanisms can be contemplated: (*i*) the induced-fit model and (*ii*) the population-shift model. According to the induced-fit model, binding of a ligand induces the conformational change in the binding site that results in a new active conformation of the enzyme (1). In other words, the enzyme assumes the shapes complementary to the substrate only after the substrate is bound. On the other hand, according to the population-shift model, in the vicinity of its native state the enzyme exists in the multiple conformations at its binding site. The ligand binds selectively to an active conformation and by that means shifts the equilibrium toward the binding conformation (2, 3). Here, we explore these two very different viewpoints of the ligand binding mechanism by investigating the allosteric conformational changes of *Escherichia coli* adenylate kinase (AdK) in the presence and absence of a ligand.

AdK is a monomeric phosphotransferase enzyme that catalyzes reversible transfer of a phosphoryl group from ATP to AMP via the reaction ATP-Mg^{2+} + AMP ↔ ADP-Mg^{2+} + ADP. The structure of AdK is composed of the three main domains, the CORE (residues 1–29, 68–117, and 161–214), the ATP binding domain called the LID (residues 118–167), and the NMP binding domain called the NMP (residues 30–67) (Fig. 1). Several crystal structures of AdK from *E. coli* and other organisms are available, both free and in complex with substrates and inhibitors (see ref. 4 and references therein). Based on structural analysis, it appears that AdK assumes an "open" conformation in the unligated structure and a "closed" conformation in a structure crystallized with an inhibitor AP_5A (5, 6), which is a bi-substrate analog inhibitor that connects ATP and AMP by a fifth phosphate and mimics both substrates (Fig. 1). Supposedly, during the transition from the "open" to "closed" form, the largest conformational change occurs in the LID and NMP domain with the CORE domain being relatively rigid. The active site pocket of AdK is lined by conserved arginine residues (Arg-36, Arg-88, Arg-123, Arg-152, and Arg-167) surrounding the negative phosphate groups of the inhibitor [supporting information (SI) Fig. 7]. These residues have been suggested to play a crucial role in the substrate binding and domain closure (7). The ATP binding site of AdK resembles that of a motor protein F1-ATPase and of a muscle protein myosin.

Abundant kinetic and thermodynamic experimental data are available for AdK (8–12). Notably, dynamic NMR dispersion experiments have shown quantitatively that the large-scale conformational change associated with the LID opening motion is rate-limiting for the overall catalysis of the enzyme (11). The conformational dynamics of AdK has also been investigated computationally, mainly in the ligand-free state, using standard MD (13), a distance replica exchange method (14), normal mode analysis with simplified elastic-network model (15–18), a minimalist plastic-network model (19), and a coarse-grained model that approximately considered ligand interactions (20). Overall, these studies have provided important insights into the functional motions of the enzyme. Still, the atomically detailed mechanism of ligand binding and the cooperativity of individual domain motions, transition states, and intermediate conformations along the pathway are not known precisely. Our goal is to explore in atomic detail the pathways between open and closed states of AdK, both in the presence and absence of the substrate and obtain the corresponding free energy profiles.

It is well known that capturing large-scale and long-time conformational transitions of biomolecules is a challenging task (21). Standard molecular dynamics simulations are limited to time scales of a few hundreds of nanoseconds. This has resulted in the development of advanced sampling methodologies to

Author contributions: K.A. and C.L.B. designed research; K.A. performed research; K.A. analyzed data; and K.A. wrote the paper.

The authors declare no conflict of interest.

This article is a PNAS Direct Submission.

*To whom correspondence should be addressed. E-mail: brooks@scripps.edu.

This article contains supporting information online at www.pnas.org/cgi/content/full/0706443104/DC1.

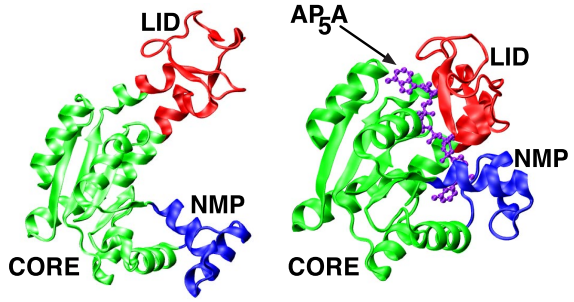

Fig. 1. Adenylate kinase in open (*Left*) and closed (*Right*) states as observed in x-ray crystal structures (5, 6).

tackle biomolecular motions that take place on longer time scales (see refs. 22–26 and references therein). Alternative methods that employ a highly simplified potential have also proved successful in modeling large-scale collective motions of biomolecules (see ref. 27 and references therein).

To accomplish our goal, we used a combination of two well established approaches, the nudged elastic band (NEB) method (28, 29) and umbrella sampling molecular dynamics simulations (30). The choice of an appropriate order parameter is important for the success of the umbrella sampling simulations. This progress coordinate should well separate the two endpoint states and otherwise provide minimal restraint on the nature of conformations adopted along the path between these states. Here, we chose the difference in root mean square deviation from the open and closed states of AdK (ΔD_{rmsd}) as an order parameter for the characterization of the conformational transition. In the past, the ΔD_{rmsd} order parameter has been applied successfully to investigating interesting biological problems (31–33). Whether this order parameter coincides with the reaction coordinate could be established by computing commuter probability distributions as put forward by Chandler and coworkers (34), but such an analysis is not pursued here. However, the ΔD_{rmsd} order parameter contains information about numerous individual degrees of freedom (e.g., the flip of side chains) that contribute to the overall conformational transition. By constructing free energy profiles along these additional degrees of freedom based on the underlying umbrella sampling in ΔD_{rmsd}, one can often gain mechanistic insights (see *Computational Methods*). The use of NEB in conjunction with sampling along the ΔD_{rmsd} reaction coordinate has not previously been employed in this context. Earlier work that used ΔD_{rmsd} as an order parameter relied on the targeted dynamics method, employing unphysical forces of an orders of magnitude greater than $k_{\mathrm{B}}T$, to generate the initial paths. NEB, on other hand, is useful for finding a minimum-energy path (MEP) connecting two local minima on the potential-energy surface and has been applied successfully to investigate transformation of several biomolecules (29, 35).

Our application of the advanced sampling methodology unravels details of AdK's conformational change pathway that tie well with the large body of experimental data as well as other modeling studies. Specifically, our calculated free energy profiles of AdK reveal that the enzyme samples a wide ensemble of conformations that differ by only few $k_{\mathrm{B}}T$, even in the absence of its substrate. The energy landscape changes upon binding to an inhibitor, and the closed conformation is predominantly favored in the ligand-bound state. The ligand binding occurs concurrently with the conformational change and toward the closed state along the pathway as determined by drawing analogy of the binding process with the idea from the Marcus theory of electron transfer (36). Overall, our results emphasize the dynamic nature of the enzyme and refine the viewpoint of the binding mechanism based on the knowledge of the static crystal structures alone. This picture is most consistent with a population-shift mechanism.

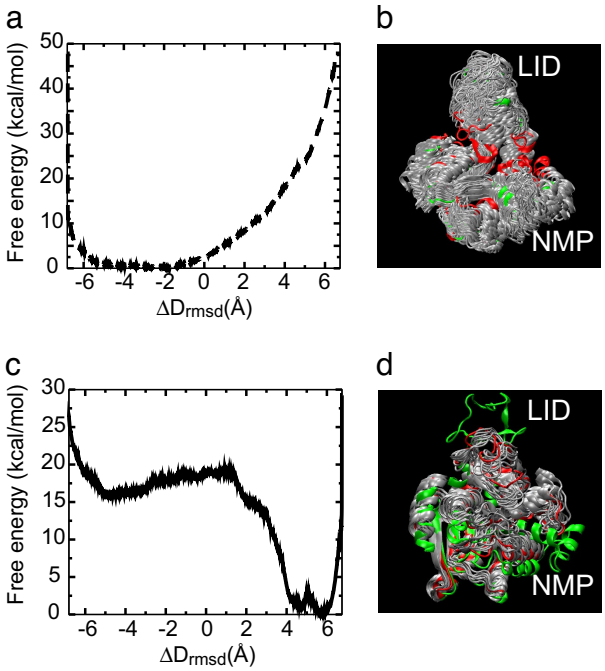

Fig. 2. Free energy profiles associated with the conformational transitions of AdK in the ligand-free and ligand-bound pathways and the corresponding ensemble of low-energy structures sampled along each path. (*a*) The one-dimensional energy profile along the ΔD_{rmsd} reaction coordinate in the ligand-free pathway. (*b*) Superimposed structures of AdK in the crystal closed (red), crystal open (green), and intermediate (silver) states within 5 kcal/mol from the global minimum in the ligand-free path. (*c*) Free energy profile associated with the conformational transitions of AdK in the ligand-bound pathway. (*d*) Superimposed structures of AdK in the crystal closed (red), crystal open (green), and intermediate (silver) states that lie within ΔD_{rmsd} range of 4–6 Å in the ligand-bound path.

Results and Discussion

Details of the Conformational Change Process in the Ligand-Free AdK. Fig. 2*a* shows the free energy profile associated with the conformational transition pathway of AdK in the ligand-free state along a one-dimensional reaction coordinate. As shown, there is a wide free energy well representing the open conformation of AdK with no significant energy barrier separating the open and closed states. Upon characterizing all of the structures along the path, based on the midpoint of the ΔD_{rmsd} range, the structures toward the right are at least 2.5 kcal/mol higher in the free energy than the lowest free energy minimum, corresponding to ΔD_{rmsd} of −1.8 Å. It is more informative to look at the two-dimensional free energy surfaces along the ΔD_{rmsd} order parameter with respect to the rmsd from the crystal open and closed states, respectively (SI Fig. 8). The free energy of the conformational change is within 5 kcal/mol up to 5.5 Å from the open state and 4 Å from the closed state. These observations suggest that AdK is a flexible molecule and assumes a wide ensemble of conformations separated by only a few $k_{\mathrm{B}}T$ around the crystallographically observed open state. Most of the enzyme's motion is concentrated in the LID and the NMP domain (Fig. 2*b*).

The domain closure of AdK has been investigated in the solution using energy transfer experiments by Sinev *et al.* (9) and recently in the laboratory of Kern (personal communication). Energy transfer studies in the laboratory of Kern were performed by labeling residues Ile-52 and Lys-145 located in the NMP and the LID domain, respectively. The broad distance

BIOPHYSICS

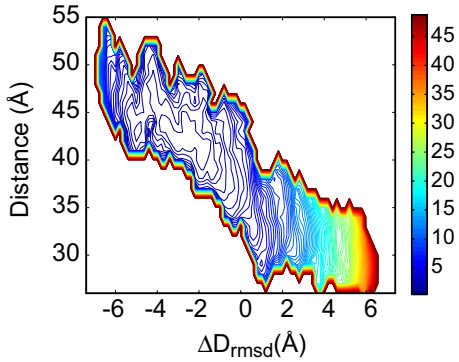

Fig. 3. Free energy surface of the distance between the mass centers of residues Ile-52 and Lys-145 and the ΔD_{rmsd} reaction coordinate. The mass center distance between the residues Ile-52 and Lys-145 is 44.8 Å and 29.7 Å in the crystal open and closed form, respectively.

distribution between the labeled residues was observed, which led to the suggestion that AdK in the ligand-free state samples a large conformational space. To mimic these experiments, we computed the free energy profile in the plane spanned by the distance between mass center of residues Ile-52 and Lys-145 along the reaction coordinate (Fig. 3). As displayed in the Fig. 3, the distance between the residues fluctuates from the 44.8 Å to 29.7 Å, corresponding to the distances observed in the unbound crystal open and inhibitor bound crystal closed states, without any large free energy barrier. Thus, these results reemphasize that even in the absence of ligand, AdK can sample conformations similar to the closed form.

However, in the energy transfer experiments, the order of individual domain motions cannot be determined. This is because when measuring the change in distance between two labeled residues, the result is a scalar and gives no indications of which residue moves. To dissect the order of domain motions, we computed the free energy profiles in the plane spanned by the mass center distance between the LID and the CORE domain, and the mass center distance between the NMP and the CORE domain along the reaction coordinate, respectively (Fig. 4). The mass centered distance between the LID and the CORE is 30.1 Å and 21.0 Å in the crystal open and closed form. The NMP and the CORE distance is 22.0 Å and 18.3 Å in the x-ray open and closed form. Interestingly, the LID domain samples conformations from the distance found for the free form (≈30 Å) to the distance found for the inhibitor bound form (≈22 Å) with almost no energy barrier (Fig. 4*a*). The NMP domain, on the other hand, samples limited conformational space in the ligand-free state with a small energetic cost (Fig. 4*b*). The complete closing of the NMP domain requires higher energy compared with the LID domain. It appears energetically that the NMP closing must follow the LID in the ligand-free state. The ordered closing of domains is in agreement with the similar suggestions from other computational work employing low-resolution models (19, 20).

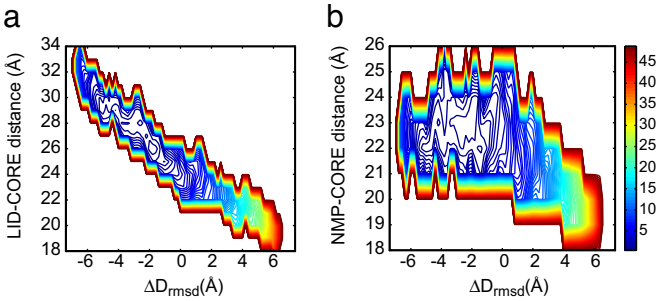

Fig. 4. Energetics of the individual LID and NMP domain closure in the ligand-free pathway. (*a*) PMF in the plane spanned by the LID-to-CORE mass center distance and the ΔD_{rmsd} reaction coordinate. (*b*) PMF in the plane spanned by the NMP-to-CORE mass center distance and the ΔD_{rmsd} reaction coordinate. The distance between the LID and the CORE center of mass is 30.1 Å and 21.0 Å in the crystal open and closed form, respectively. The NMP and the CORE distance is 22.0 Å and 18.3 Å in the x-ray open and closed form, respectively.

Conformational Change Pathway of AdK Bound to an Inhibitor. Fig. 2*c* shows the free energy profile associated with the conformational transition pathway of AdK bound to an inhibitor. Two main characteristics are evident in the free energy profile. First, there is almost no energy barrier separating the open to closed states. Second, there is a deep free energy well in the closed state (ΔD_{rmsd} value of 4–6 Å), but the open ligand-bound state is only marginally stable. This free energy well is narrower than that observed for the open state in the unligated pathway, suggesting the dampening of the enzyme's motions upon binding the inhibitor. Clearly, the conformational change is affected by the binding of the ligand because there is no well defined minimum in the closed state for the unligated pathway of AdK. In SI Fig. 9, we show the two-dimensional free energy surfaces spanned by rmsd from the crystal open and closed state along the reaction coordinate, respectively. All structures up to 6 Å from the crystal open state (see SI Fig. 9*a*) and 3 Å from the crystal closed state (SI Fig. 9*b*) are much higher in energy compared with the completely closed form, and there is a free energy minimum beyond 6 Å from the open conformer. Most likely, the energy minimum corresponds to the low energy structures resulting from the formation of the favorable interactions between the ligand and protein residues. On comparing the energy profiles of the ligand-bound and -unbound pathway, we can safely conclude that in the ligand-unbound state, the open form is the most stable form of the enzyme. In the same way, the closed form corresponds with the ligand-bound state.

Local Conformational Changes. The active site cleft of AdK is lined with several conserved arginine residues (Arg-36, Arg-88, Arg-123, Arg-156, and Arg-167), which surround the phosphate groups of the inhibitor (SI Fig. 7). It is believed that these residues help stabilize the negative charge on the phosphates. Some of these arginines have been shown to participate in phosphate binding and catalysis (37, 38). We analyzed the motion of the arginine residues by monitoring its torsion angle (C^{δ}-C^{γ}-N^{ε}-C^{ζ}) in both ligand-bound and -unbound pathways. The results are summarized in Fig. 5. As shown, all residues sample quite similar conformational space up to a ΔD_{rmsd} of 3.0 Å in the corresponding pathways. However, in the ligand-bound pathway, motion of residues past ΔD_{rmsd} of 3 Å is restricted to a narrow range of dihedral angle values. These observations suggest that even in the absence of the ligand, the enzyme exists in its multiple conformations, including an active conformation, at its binding site. The ligand binds selectively to an active conformation and shifts the preexisting equilibrium of different conformational states toward the bound conformation. The energy required to align the catalytic groups for the transition state is accessible via thermal fluctuations in the ligand-free state.

Activation Energy Barrier. Dynamic NMR experiments suggest that the motion of the domains is an activated process and rate-limiting in the overall kinetic pathway (11). On the contrary, our simulations of the ligand-bound AdK, where the substrate was placed in the active site of the open state, show that the enzyme undergoes a barrierless transition from the open to closed state. Furthermore, there is no well defined minimum

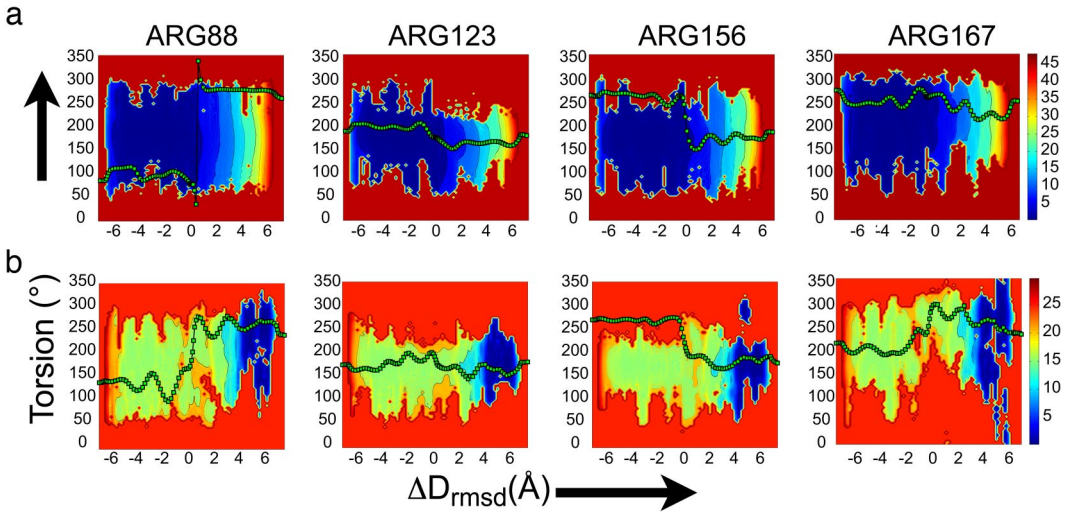

Fig. 5. Local conformational changes associated with the large-scale domain motions of AdK. Free energy surfaces along ΔD_{rmsd} (abscissa) and torsion angle (C^{δ}-C^{γ}-N^{ε}-C^{ζ}) of the conserved arginine residues Arg-88, Arg-123, Arg-156, and Arg-167 (ordinate) in the ligand-free (*a*) and ligand-bound (*b*) pathways. The solid line represents the evolution of the dihedral angle (C^{δ}-C^{γ}-N^{ε}-C^{ζ}) associated with the rotation of arginine residues as obtained from the optimized NEB path.

toward the ligand-bound open state. Together, these observations indicate that the ligand does not bind effectively to an open conformation of the enzyme but somewhere later along the pathway. The region where the binding process occurs is suggested by drawing analogy between the ligand binding process to the idea from the Marcus electron transfer theory (36). Theoretically, the binding occurs at the intersection region of the free energy surfaces of the ligand-bound state and the ligand-unbound state. To find where the binding event would occur, the one-dimensional free energy profile of the ligand-unbound pathway is superimposed on the energy profile from the ligand-bound pathway (Fig. 6). The two profiles are defined by using a similar reaction coordinate (ΔD_{rmsd}), and the equilibrium free energy of the open and closed conformers is set to zero. It is clear from Fig. 6 that the transition state region lies far toward the closed state. Thus, the substrate binds favorably to the closed like conformations where protein residues are better aligned to interact with it. Significantly, the estimated activation energy barrier along the closing pathway is ≈12.5 kcal/mol. This value is lower but comparable to the barrier estimate from the rate of the reaction (13.2–14.2 kcal/mol), as obtained from experimental kinetic data [k_{close}, domain closing rate of 1,374 s^{-1}, and k_{cat}, the overall rate of catalysis of 263 s^{-1} (11)]. Our estimated free energy values suggest that the rate-limiting step is associated with the complete closing of the domains and is in excellent agreement with experiments. Specifically, closing of the NMP domain is slow because the LID domain and catalytic residues can sample active conformations even in the ligand-free state as discussed above.

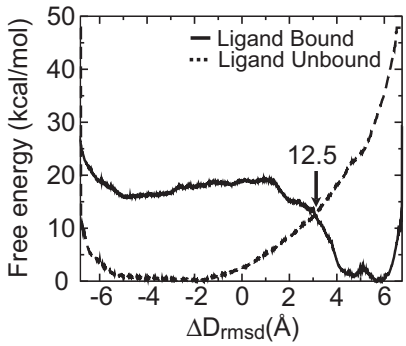

Fig. 6. Superimposed one-dimensional free energy profile of the ligand-unbound pathway and the energy profile from the ligand-bound pathway. The intersection region of the two profiles locates the transition state of the conformational transition. The stability of the open unbound and closed bound state is assumed to be the same.

To determine the transition-state region, information about the relative stability of the open and closed forms is required. While determining the activation free energy (Fig. 6), we assumed the equilibrium free energy of the unbound open and bound closed structures to be equal, but other scenarios where the relative stability of the conformers is different can be envisioned (18). The experimentally determined standard binding free energy of ATP and AMP is -6.3 ± 0.9 and -4.6 ± 0.3 kcal/mol, respectively (39). Because the inhibitor AP_5A is a combination of ATP and AMP, its total binding energy is approximately equal to the sum of the binding energy of its individual components (40), which is approximately -11.0 kcal/mol. Under the assumption that ligand binding is fast compared with the conformational change, depending on the concentration of the substrate, the effective binding free energy of the inhibitor (AP_5A) can be varied within a few kcal/mol. For example, if the closed conformation is 1 kcal/mol more stable than the open state, as suggested from FRET experiments (D. Kern, personal communication), the resulting activation energy barrier of 12.3 kcal/mol for closing and 13.3 kcal/mol for opening is in reasonable agreement with the experiments.

Conclusions

We explored the conformational change process associated with ligand binding by investigating transitions of AdK in the presence and absence of the ligand. According to the static crystal view, in the ligand-free state, AdK exists in its open state; i.e., open LID and NMP domain. The inhibitor binds in the open state and then the closed state is achieved. Our energetic and dynamic analysis of AdK's conformational change process suggests a different scenario for the ligand binding. Even in the absence of the ligand, the protein domains and the key binding arginine residues in the active site undergo dynamic interchange between the open and near closed conformations. The ligand binds toward the closed state where the catalytic groups are favorably aligned to interact with the incoming ligand. After the substrate is captured, small conformational rearrangements follow, and

the ligand-bound form becomes energetically most favored. Energetically, the entire conformational change process can be described as the transformation of the enzyme from the free energy surface related with the ligand-free form to that of the ligand-bound form upon binding the inhibitor. Our estimated activation energy barriers and the existence of the ensemble of conformational states in the ligand-free state are in line with the solution and NMR experiments.

Computational Methods

To delineate atomically detailed pathways for AdK's conformational transitions, we first generated two initial paths, with and without inhibitor, between the open and closed states of AdK using the NEB method. Subsequently, each configuration along the path was subjected to umbrella sampling MD simulations with restraints on the ΔD_{rmsd} order parameter. The CHARMM program (c33a1 version) (41) with the all-atom CHARMM22/CMAP force field was used for all calculations (42, 43).

System Preparation. In total, four reference structures of AdK were used to generate two paths, one with and the other without the inhibitor bound to it. The two end-point reference structures for generating initial paths are the known crystal coordinates of *E. coli* AdK in the open state without bound inhibitor (PDB entry 4AKE) and in the closed state with bound inhibitor (PDB entry 1AKE) (5). To investigate the binding mechanism, two other states, open state with inhibitor and closed state without inhibitor, were modeled based on the crystal conformations. The open state was modified by positioning an inhibitor (AP_5A) in the active site after superimposing heavy atoms in the open and closed forms. The side chain of Arg-88 was rotated slightly to prevent steric clashes with the inhibitor. The closed state was modified by simply removing the inhibitor from the binding site. Hydrogen atoms were added to heavy atoms by using the CHARMM HBUILD facility (44). Each structure was then minimized for 100 steps of adapted basis Newton–Raphson (ABNR) and steepest descent (SD) minimization with a large harmonic restraint. These four reference structures were used for the subsequent simulations.

Initial Paths. To generate initial configurations for umbrella sampling, the NEB method implemented in CHARMM (29) was used. Specifically, we used NEB to find MEP between open and closed states of AdK in the presence and absence of an inhibitor. For the path without inhibitor, the two reference structures were the crystal open state and the modified closed state without inhibitor. A total of 81 replicas including the end-point states were used to describe the conformational transition. Initial structures were generated by linear interpolation between the end-point states. Then, the initial path was minimized with 500 SD steps using the replica path method with a spring constant of 500,000 kcal/mol/Å^2 without NEB force projection. The resulting path was minimized with NEB by using ABNR minimization for 2,000 steps with the force constant of 10,000 kcal/mol/Å^2. A final RMS off-path force of 0.002 kcal/mol/Å^2 was reached. Further minimization did not change the gradient significantly. A distance-dependent dielectric coefficient (RDIE) was used to approximate solvent screening without including explicit water molecules. Electrostatic and van der Waals interactions were truncated at 16 Å. A similar protocol was used to generate a minimum energy path with an inhibitor bound to AdK. To compute the free energy profiles along the conformational change path, umbrella sampling MD simulations were performed as described below.

Umbrella Sampling Simulations. The initial structures obtained from the NEB path were used as starting points for umbrella sampling MD simulations. The sampling was performed with the restraint w_j on the ΔD_{rmsd} order parameter (31):

$$w_j = K_{\mathrm{rmsd}}(\Delta D_{\mathrm{rmsd}} - \Delta D_{\mathrm{min}})^2, \qquad [1]$$

where ΔD_{min} is the value around which ΔD_{rmsd} is restrained, and K_{rmsd} is the force constant. The ΔD_{rmsd} order parameter is the difference in rmsd values of each structure from the reference reactant and product states. It is described as follows:

$$\Delta D_{\mathrm{rmsd}} = \mathrm{rmsd}(X_t, X_{\mathrm{open}}) - \mathrm{rmsd}(X_t, X_{\mathrm{closed}}), \qquad [2]$$

where X_t is the instantaneous structure during simulation, and X_{open} and X_{closed} are the two reference open and closed states of AdK, respectively.

The 81 structures obtained from the NEB path optimization cover an rmsd range of 7.2 Å. Structures are separated by the interval of 0.2 Å in the ΔD_{rmsd} order parameter space. These 81 structures formed 81 windows for umbrella sampling runs. In each window, the structure was subjected to restrained minimization using SD minimization for 1,000 steps followed by ABNR minimization for 500 steps. During minimization, a large harmonic restraint of 250 kcal/mol/Å^2 was applied on protein heavy atoms to prevent the structures from drifting far from the starting configurations. Then, equilibration was performed with the restraint (Eq. **1**) on protein heavy atoms, where the force constant was reduced from 210 kcal/mol/Å^2 to 10 kcal/mol/Å^2 over a period of 75 ps of constant temperature and volume MD simulation. After the equilibration, production dynamics was performed and the structures were allowed to evolve with a weak one-dimensional ΔD_{rmsd} restraint of 10 kcal/mol/Å^2 on protein heavy atoms for 525 ps.

Equilibration and production dynamics was performed at constant temperature (300 K) by using Langevin dynamics. The SHAKE algorithm was used to constrain the bonds involving hydrogen atoms. This allowed the use of an intermediate time step of 0.0015 ps with the leapfrog integrator. The Langevin collision parameter of 10 ps^{-1} was chosen to couple the system to a 300 K heat bath. Electrostatic and van der Waals interactions were truncated at 16 Å with a switch function. The solvent effects were modeled through the GB/SA solvation scheme (45, 46). Within this scheme, the electrostatic part of the solvation energy is computed from the generalized Born (GBMV) approximation. The Born radii were obtained by using analytical method II available in CHARMM (41).

The weighted histogram analysis method (WHAM) (47) was used to obtain the potential of mean force along the one-dimensional ΔD_{rmsd} reaction coordinate from the time series of the ΔD_{rmsd} variable saved every time-step of 525 ps production dynamics. The two-dimensional free energy profile along other additional degrees of freedom was generated by using trajectories from the umbrella sampling MD simulations (31). For example, the PMF surface as a function of the two-dimensional reaction coordinates defined by ΔD_{rmsd} and $\mathrm{rmsd}(X_t - X_{\mathrm{closed}})$ was obtained by considering the biased probability distribution $\rho_{\mathrm{bias}}(\zeta_1, \zeta_2)$, where, $\zeta_1 = \mathrm{rmsd}(X_t - X_{\mathrm{closed}})$ and $\zeta_2 = \Delta D_{\mathrm{rmsd}}$. The unbiased probability distribution $\rho(\zeta_1, \zeta_2)$ was by obtained by using the standard WHAM approach. Convergence of the free energy calculations was tested by extending the production dynamics for another 150 ps (data not shown). There was no significant change in the free energy estimates from longer runs.

This work was supported by the National Institutes of Health (Grants RR12255 and GM48807) and the Center for Theoretical Biological Physics (CTBP) through funding from the National Science Foundation (Grant PHY0216576). K.A. thanks the La Jolla Interfaces in Science Interdisciplinary Program, sponsored by the Burroughs Wellcome Fund, for financial support through their postdoctoral fellowship programs.

1. Koshland DE, Jr (1958) *Proc Natl Acad Sci USA* 44:98–104.
2. Koshland DE, Jr, Nemethy G, Filmer D (1966) *Biochemistry* 5:365–385.
3. Volkman BF, Lipson D, Wemmer DE, Kern D (2001) *Science* 291:2429–2433.
4. Vonrhein C, Schlauderer GJ, Schulz GE (1995) *Structure* 3:483–490.
5. Muller CW, Schulz GE (1992) *J Mol Biol* 224:159–177.
6. Muller CW, Schulz GE (1993) *Proteins* 15:42–49.
7. Yan HG, Dahnke T, Zhou BB, Nakazawa A, Tsai MD (1990) *Biochemistry* 29:10956–10964.
8. Dahnke T, Shi Z, Yan H, Jiang RT, Tsai MD (1992) *Biochemistry* 31:6318–6328.
9. Sinev MA, Sineva EV, Ittah V, Haas E (1996) *Biochemistry* 35:6425–6437.
10. Shapiro YE, Sinev MA, Sineva EV, Tugarinov V, Meirovitch E (2000) *Biochemistry* 39:6634–6644.
11. Wolf-Watz M, Thai V, Henzler-Wildman K, Hadjipavlou G, Eisenmesser EZ, Kern D (2004) *Nat Struct Mol Biol* 11:945–949.
12. Shapiro YE, Meirovitch E (2006) *J Phys Chem B* 110:11519–11524.
13. Lou H, Cukier RI (2006) *J Phys Chem B* 110:12796–12808.
14. Lou H, Cukier RI (2006) *J Phys Chem B* 110:24121–24137.
15. Tama F, Brooks CL, III (2002) *J Mol Biol* 318:733–747.
16. Miyashita O, Onuchic JN, Wolynes PG (2003) *Proc Natl Acad Sci USA* 100:12570–12575.
17. Temiz NA, Meirovitch E, Bahar I (2004) *Proteins* 57:468–480.
18. Miyashita O, Wolynes PG, Onuchic JN (2005) *J Phys Chem B* 109:1959–1969.
19. Maragakis P, Karplus M (2005) *J Mol Biol* 352:807–822.
20. Whitford PC, Miyashita O, Levy Y, Onuchic JN (2007) *J Mol Biol* 366:1661–1671.
21. Schlick T (2002) *Molecular Modeling and Simulation: An Interdisciplinary Guide* (Springer, New York).
22. Brooks CL, III (2002) *Acc Chem Res* 35:447–454.
23. Karplus M, McCammon JA (2002) *Nat Struct Biol* 9:646–652.
24. Karplus M, Kuryian J (2005) *Proc Natl Acad Sci USA* 102:6679–6685.
25. Arora K, Schlick T (2005) *J Phys Chem B* 109:5358–5367.
26. Khavrutskii IV, Arora K, Brooks CL, III (2006) *J Chem Phys* 125:174108.
27. Tama F, Brooks CL, III (2005) *Annu Rev Biophys Biomol Struct* 35:115–133.
28. Jónsson H, Mills G, Jacobsen KW (1998) in *Classical and Quantum Dynamics in Condensed Phase Simulations*, eds Berne B, Ciccoti G, Coker DF (World Scientific, Singapore), pp 385–404.
29. Chu JW, Trout BL, Brooks BR (2003) *J Chem Phys* 119:12708–12717.
30. Torrie GM, Valleau JP (1977) *J Comput Phys* 23:187–199.
31. Banavali NK, Roux B (2005) *J Am Chem Soc* 127:6866–6876.
32. Banavali NK, Roux B (2005) *Structure* 13:1715–1723.
33. Yu H, Ma L, Yang Y, Cui Q (2007) *PLoS Comput Biol* 3:e23.
34. Bolhuis PG, Chandler D, Dellago C, Geissler PL (2002) *Annu Rev Phys Chem* 53:291–318.
35. Mathews DH, Case DA (2006) *J Mol Biol* 357:1683–1693.
36. Marcus RA, Sutin N (1985) *Biochim Biophys Acta* 811:265–322.
37. Burlacu-Miron S, Gilles AM, Popescu A, Barzu O, Craescu CT (1999) *Eur J Biochem* 264:765–774.
38. Sheng XR, Li X, Pan XM (1999) *J Biol Chem* 274:22238–22242.
39. Sanders CR, II, Tian GC, Tsai MD (1989) *Biochemistry* 28:9028–9043.
40. Parang K, Till JH, Ablooglu AJ, Kohanski RA, Hubbard SR, Cole PA (2001) *Nat Struct Biol* 8:37–41.
41. Brooks BR, Bruccoleri RE, Olafson BD, States DJ, Swaminathan S, Karplus M (1983) *J Comput Chem* 4:187–217.
42. MacKerell AD, Jr, Bashford D, Bellott M, Dunbrack R, Jr, Evanseck J, Field M, Fischer S, Gao J, Guo H, Ha S, *et al.* (1998) *J Phys Chem B* 102:3586–3616.
43. MacKerell AD, Jr, Feig M, Brooks CL, III (2004) *J Am Chem Soc* 126:698–699.
44. Ryckaert JP, Ciccotti G, Berendsen HJC (1977) *J Comput Chem* 23:327–341.
45. Lee MS, Salsbury FR, Jr, Brooks CL, III (2002) *J Chem Phys* 116:10606–10614.
46. Lee MS, Feig M, Salsbury FR, Jr, Brooks CL, III (2003) *J Comput Chem* 24:1348–1356.
47. Kumar S, Bouzida D, Swendsen RH, Kollman PA, Rosenberg JM (1992) *J Comput Chem* 13:1011–1021.